Refining the chain-branching process in the low-temperature oxidation of 1-hexene with synchrotron-based PEPICO spectroscopy

Jérémy Bourgalais, Caroline Smith Lewin, Olivier Herbinet, Gustavo Garcia, Philippe Arnoux, Luc-Sy Tran, Guillaume Vanhove, Laurent Nahon, Frédérique Battin-Leclerc

Refining the chain-branching process in the low-temperature oxidation of 1-hexene with synchrotron-based PEPICO spectroscopy

Jérémy Bourgalais[1,*], Caroline Smith Lewin[1], Olivier Herbinet[1], Gustavo A. Garcia[2], Philippe Arnoux[1], Luc-Sy Tran[3], Guillaume Vanhove[3], Laurent Nahon[2], and Frédérique Battin-Leclerc[1]

[1]Université de Lorraine, CNRS, LRGP, F-54000 Nancy, France.

[2]Synchrotron SOLEIL, L'Orme des Merisiers, Départementale 128, 91190 St Aubin, France.

[3]Université de Lille, CNRS, PC2A, F-59000 Lille, France

* Corresponding author:

J. Bourgalais: jeremy.bourgalais@cnrs.fr

ABSTRACT

Understanding the chemical reactions that occur during the low-temperature oxidation of alkenes is crucial for developing advanced energy conversion devices, as alkenes are significant components of realistic fuels. Despite extensive experimental and theoretical studies, the oxidation chemistry of alkenes remains less understood compared to that of alkanes. The present study investigates the low-temperature oxidation of 1-hexene in a jet-stirred reactor, using synchrotron-based PEPICO spectroscopy at a fixed temperature (T = 625 K) and an equivalence ratio ($\phi = 0.5$). Previous studies in the literature have suggested that the discrepancy between experiments and predictions from kinetic models might be due to the kinetics considered for the chain branching process. The sensitivity of the PEPICO technique to molecular structure allowed for a comprehensive examination of the conformational landscape, facilitating the differentiation of isomers among the main intermediates: hydroperoxides, cyclic ethers, and ketohydroperoxides. Other intermediates and primary products were also quantified and compared to the predictions of a kinetic model from the literature. The results confirm that kinetic models overpredict the formation of hydroxyl ketohydroperoxides and that alkenyl hydroperoxides are the primary chain-branching agents during 1-hexene oxidation. This work underscores the need for a reassessment of the branching ratio between O_2-addition and the isomerization of hydroxy alkyl radicals.

KEYWORDS:

Alkene oxidation | Jet-stirred reactor | synchrotron radiation | photoelectron spectroscopy | kinetic modeling

ABBREVIATIONS:

low temperature oxidation, LTO; ketohydroperoxides, KHPs; hydroxyl cyclic ethers, HyCE; alkenyl cyclic ethers, AnCE; alkenyl ketohydroperoxides, AnKHP; hydroxyl ketohydroperoxides, HyKHP; jet-stirred reactor, JSR; gas chromatography, GC; mass spectrometry, MS; synchrotron vacuum ultraviolet photoionization, SVUV-PIMS; total ion yield, TIY; adiabatic ionization energy, AIE; photoionization cross sections, PICS; synchrotron-based photoelectron photoion coincidence, SVUV-PEPICO; threshold photoelectron

spectrum, TPES; velocity map imaging, VMI; density functional theory, DFT; time-independent adiabatic Hessian Franck-Condon, TI-AH|FC.

NOVELTY AND SIGNIFICANCE STATEMENT

In the context of the development of detailed chemical kinetic model for the design of advanced energy conversion devices, this work involves utilizing synchrotron-based photoelectron spectroscopy to identify and quantify intermediates during the low-temperature oxidation of 1-hexene in a jet-stirred reactor. By thoroughly examining the conformational landscape and effectively distinguishing between isomers, comparisons with current kinetic models from the literature indicate the need for a reevaluation of the chain-branching process.

AUTHOR CONTRIBUTIONS

JB, OH, CSL, PA, LST, GV, and FBL collected the experimental data. GAG and LN provided support for the analysis. JB performed the theoretical calculations, analyzed the data, and wrote the original draft. All the authors contributed to review the final manuscript.

I. INTRODUCTION

Alkenes constitute a significant portion of practical fuels, making up to 20% of the total volume in gasoline blends, depending on the composition and source of crude oil [1]. In the pursuit of developing cost-effective and environmentally friendly combustion processes, it is crucial to comprehend the chemical reactions occurring during the low-temperature oxidation (LTO) of alkenes. Moreover, the unsaturated nature of alkenes causes their chemistry to differ from that of alkanes, necessitating an understanding of the impact of this unsaturation on auto-ignition. Despite extensive experimental and theoretical studies, the LTO chemistry of long-chain alkenes with at least five carbon atoms is less well-understood compared to alkanes [2–10]. Consequently, the comprehension of the chain branching mechanism triggered by the decomposition of intermediates, such as ketohydroperoxides (KHPs), and its influence on the ignition delay during alkene LTO remains limited.

1-hexene is commonly employed as a representative alkene in surrogate fuels designed for gasoline [11]. Numerous studies have extensively explored its oxidation chemistry across a broad spectrum of temperatures and pressures, utilizing various laboratory facilities such as shock tubes, rapid compression machines, and jet-stirred reactors [3,4,6,8,12–16]. The LTO of 1-hexene (EH) primarily follows two pathways: H-abstraction and OH-addition onto the double bond of the carbon chain. These pathways lead to the formation of alkenyl radicals, mainly allylic (E) and hydroxy alkyl radicals (ROH), respectively (see Figure 1). Analogous to alkane LTO, these radicals undergo a sequence of reactions, including O_2-addition, H-shift, and decomposition. These reactions culminate in the formation of hydroxyl cyclic ethers (HyCE, m/z 116), alkenyl cyclic ethers (AnCE, m/z = 98), alkenyl ketohydroperoxides (AnKHP, m/z 130), and hydroxyl ketohydroperoxides (HyKHP, m/z 148). The reactivity of 1-hexene at low temperatures is controlled by the delicate balance between the formation of KHPs, which act as chain branching agents, the Waddington mechanism [17] (a crucial chain propagation channel that promotes aldehyde formation), and the formation of CEs.

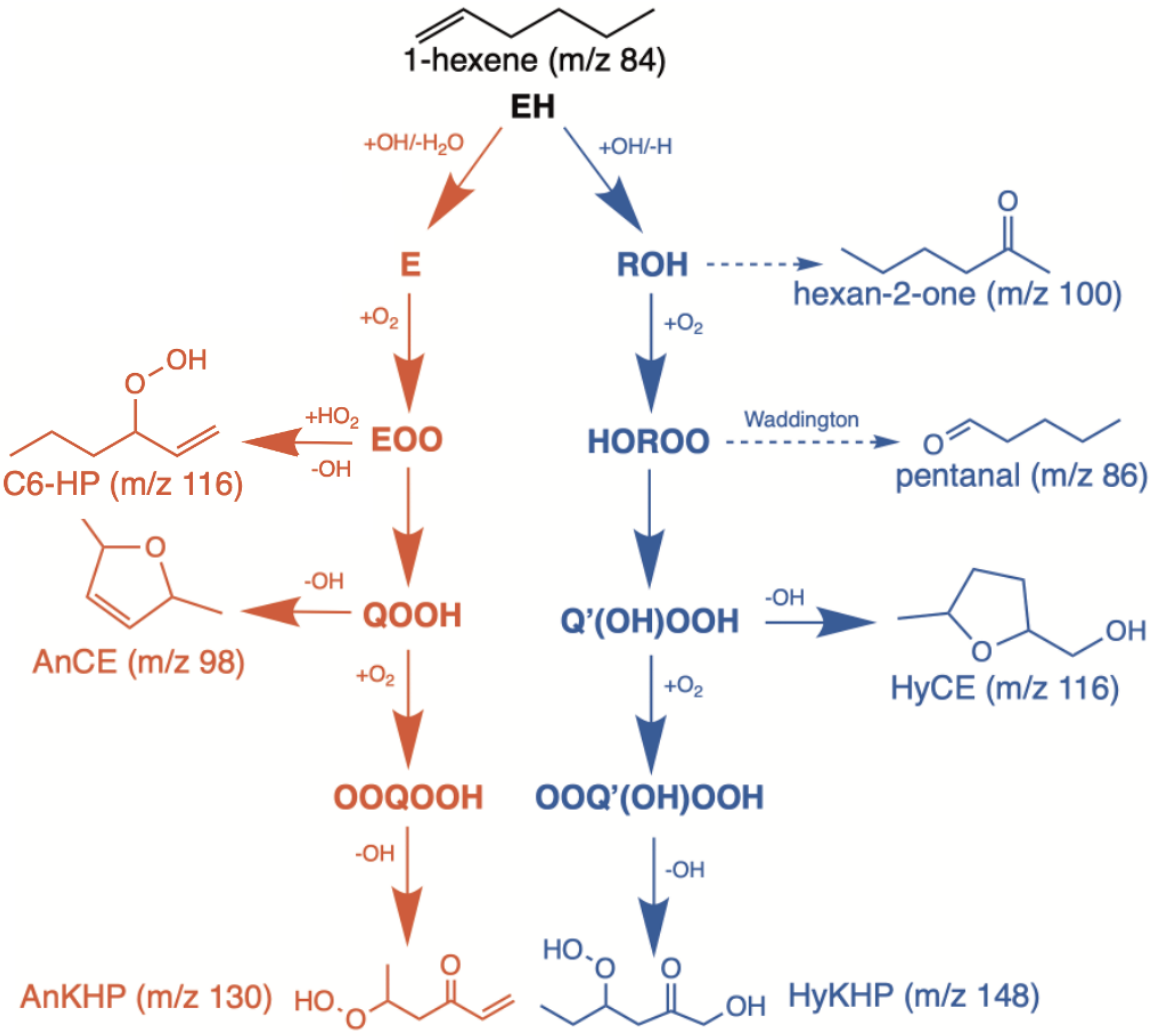

Figure 1. Simplified scheme of the two main reaction pathways in the LTO of 1-hexene showing a non-exhaustive list of the isomers detected in this work. Only the products of interest in this work are represented. The dotted arrows refer to more than one reaction step and co-products are not displayed for the sake of clarity.

Battin-Leclerc et al. [3] were the first to use a near-atmospheric jet-stirred reactor (JSR) coupled to a time-of-flight mass spectrometer with synchrotron vacuum ultraviolet photoionization (SVUV-PIMS) to detect elusive intermediates in the LTO of 1-hexene [3]. They compared the ionization threshold of the total ion yield (TIY) curve of m/z 116 to the calculated adiabatic ionization energy (AIE) of the most expected CE isomers and 3-hydroperoxyhex-1-ene (C6-HP). The AIE analysis suggested that C6-HP formation, by combination of E and HO_2 radicals, would be favored over HyCEs, formed by O_2 addition to the radical obtained by OH-addition to the fuel. Battin-Leclerc et al. [3] suggested that the non-observation of HyCEs might be due to dissociative ionization, a view now contradicted by the understanding that only hydroperoxides are prone to strong fragmentation upon

photoionization [18,19]. However, Battin-Leclerc et al. [3] noted that the shape of the temperature evolution of the signal at m/z 116 supported the possible presence of HyCEs above 700 K; in the same work, they also quantified a HyCE (5-methyltetrahydrofuran-2-yl)methanol) by gas chromatography (GC) with mass spectrometry (MS) identification.

In subsequent work by the same team, Meng et al. [4] compared experimental measurements of mole fractions of products to predictions from their detailed kinetic model. They found that HyCEs were relatively well predicted, while C6-HP was overpredicted by a factor of 6, with a predicted C6-HP/HyCE mole fraction ratio of $\sim$0.1 at 625 K.

Dong et al. [6] conducted a more recent study with a new kinetic model, demonstrating that CEs are key species in the LTO of 1-hexene. Their kinetic model also predicts that chain branching mainly occurs via the formation of HyKHP over AnKHP, with a AnKHP/HyKHP ratio < 1, in agreement with Meng et al.'s kinetic model [4]. However, no experimental evidence of HyKHP formation was provided in Meng et al. [4].

Recently, Xie et al. [8] detected a signal at m/z 148 using a similar JSR-SVUV-PIMS setup as Battin-Leclerc et al. [3], but with a more sensitive mass spectrometer than in the 2014 study. They estimated an AnKHP/HyKHP ratio by adding the signals at the masses corresponding to those of KHPs (M) as well as their main fragments (M-33 amu). They assumed that the photoionization cross sections (PICS) were similar for both types of KHPs and that the loss of OOH was the main fragmentation pathway [20,21]. They found an experimental AnKHP/HyKHP ratio $\sim$4, showing that the kinetic models from the literature significantly underpredict the formation of AnKHP. By comparing the ionization threshold of the TIY curves of m/z 130 and m/z 148 with the calculated AIE of the isomers predicted by the kinetic models, they differentiated between KHP isomers. However, the ionization thresholds did not match the most anticipated KHPs according to the predictions of the kinetic models, suggesting an incomplete understanding of the chain branching mechanisms.

Accurately distinguishing between KHP isomers in SVUV-PIMS requires precise ionization energy calculations. However, none of the aforementioned studies included a comprehensive conformational analysis, essential for floppy molecular systems such as KHPs, whose population might be distributed over several thermally accessible conformers. The conformational landscape of the molecule can have a significant impact on the ionization energy (IE), with IEs spanning a range of over more than 1.5 eV [19] in a typical

KHP such as 3-hydroperoxybutal. This contradicts the 100 meV uncertainty assumed in Xie et al. [8].

The present study aims, for the first time, to utilize synchrotron-based photoelectron photoion coincidence (SVUV-PEPICO) spectroscopy in conjunction with high-level theoretical quantum calculations to investigate the low-temperature branching mechanism involved in the oxidation of 1-hexene. The SVUV-PEPICO technique offers enhanced structural sensitivity for analyzing complex mixtures by employing mass-selected photoelectron spectroscopy [22]. This approach provides an electronic isomer-sensitive footprint that supplements mass spectrometry, adding a new dimension to the analysis. A comprehensive review of this method's application in combustion studies has been presented by Hemberger et al. [23].

The experiments conducted in this study were carried out using a JSR, with specific conditions optimized for detecting KHPs. These conditions were closely aligned with the operating parameters utilized by Xie et al. [8]. To record the threshold mass-selected photoelectron spectra (TPES) of the intermediates and products, the JSR was coupled to the DELICIOUS III spectrometer of the VUV DESIRS beamline, located at the SOLEIL synchrotron in Saint-Aubin, France. Subsequently, the TPES were analyzed through conformer-dependent electronic structure and energy calculations. This analytical process enabled the identification and quantification of the main intermediates present under specific experimental conditions (ϕ = 0.5 and T = 625 K), facilitating a comparison with predictions from a detailed kinetic model.

II. EXPERIMENTAL AND THEORETICAL METHODS

Experimental procedure

The experimental setup employed in this study closely follows the description provided in Bourgalais et al. [24–26], with only pertinent details presented herein. A lean reactive gas mixture of 1-hexene, O_2, and He was continuously fed into a JSR operating at near-atmospheric pressure. The liquid fuel was uniformly mixed with the gas flow and evaporated, using He as the carrier gas, through a controlled evaporator mixer upstream of the JSR. The inlet flow rates were adjusted to maintain a constant temperature of 625 K (1-hexene: 1.44 g/h, O_2: 115 Nml/min, and He: 0.516 Nl/min), a specific equivalence ratio (ϕ =

0.5), and a residence time (τ = 2.5 s), parameters similar to those used in previous studies. The inlet mole fraction of the fuel was set to 0.01.

The heated JSR was located within the permanent end-station of the SAPHIRS chamber [27], situated at one of the monochromatized branches of the DESIRS VUV beamline at the SOLEIL synchrotron [28]. The gas mixture within the JSR was sampled via a micrometer pinhole, creating a molecular-beam expansion in the vacuum chamber ($\sim 10^{-4}$ mbar), connected through two consecutive skimmers to the ionization chamber. This expansion created cooled molecular beam where reactive collisions were minimized due to low number density and dilution with a carrier gas (He). Consequently, reactive intermediates were preserved during the expansion and traveled collision-free to the ionization chamber.

In the ionization chamber, the VUV synchrotron light was focused on the gas mixture, leading to the production of photoelectrons and photoions detected in coincidence using the double-imaging photoelectron/photoion (i^2PEPICO) spectrometer DELICIOUS III [29]. These particles traveled in opposite directions, dispersing based on their respective kinetic energies before reaching the velocity map imaging (VMI) spectrometer and forming concentric rings. The arrival times of the dispersed particles were recorded, and by selecting the electron arrival time as the reference time for time-of-flight detection of the photoion, mass spectra could be plotted. With photoion-mass selection, the VMI system allowed the construction of a two-dimensional matrix of mass-selected photoelectron spectra (PES) as a function of photon energy [30] using an Abel inversion technique. By selecting a specific kinetic energy range (100 meV in this work) the corresponding TPES could be obtained, here within a photon energy range from 8.5 to 10.5 eV, with a step size of 10 meV and an acquisition time of 60 s per step. The error bars in TPES were obtained by assuming a Poisson distribution of the photoelectron image pixel counts, which is propagated through the image Abel inversion transformation using standard error propagation formulae. In TPES, the signal-to-noise ratio is influenced by the number of false coincidences, when more two or more ionization events arrive too close in time. This false coincidence background leads to a uniform background in the mass spectrum but can hinder the detection of minor species when the true coincidence signal becomes commensurate with the Poisson noise of the background.

Theoretical calculations

In this study, the Merck molecular force field MMFF94 approach was employed to generate the initial structures of the conformers [31], which were then optimized at a higher level of theory using density functional theory (DFT) with the M06-2X-D3 functional [32]. The DFT functional was combined with the aug-cc-pVTZ Dunning's correlation consistent basis set [33], augmented with diffuse functions, and the zero-damped D3 dispersion correction by Grimme et al. [34] was applied to M06-2X. The optimized structures of the neutral species were used as the initial structures for the cationic forms. Two-electron integrals with tight optimization criteria were utilized to ensure the reliability of the conformer energies and vibrational frequencies, computed within the harmonic approximation at the same level of theory.

The optimized individual structures were subjected to conformational averaging using Boltzmann weighting based on electronic energies and the JSR temperature of 625 K. In this work, all reactants and products are assumed to reach equilibrium at 625 K, and the distribution of conformers remains unchanged after the expansion through the pinhole. To simulate transitions between vibrational levels of the lowest-energy neutral conformers and their cations, the time-independent adiabatic Hessian Franck-Condon (TI-AH|FC) model was used at 625 K [35]. The resulting stick spectrum was convolved with a Gaussian profile with a 200 cm^{-1} bandwidth to match the experimental resolution. The calculation of the AIEs was performed at the CBS-QB3 level of theory from the ground state of both neutral and cationic species, using optimized DFT structures [36,37]. The 0-0 transition of the computed stick spectra was adjusted to match the experimental spectra within the uncertainty of the energy calculation.

It should be noted that when dealing with flexible molecular structures like hydroperoxides, the analysis of TPES presents challenges arising from the presence of vibrational modes characterized by low frequencies, which often lead to limited overlaps between vibrational wavefunctions washing out the vibrational information which, combined with a low signal-to-noise ratio with possibly some spurious peaks and a notable number of potential isomers, make individual assignments challenging. Therefore, while simulated spectra can assist in extracting critical features from experimental spectra, they might not encompass all potential molecular structures.

III. RESULTS AND DISCUSSION

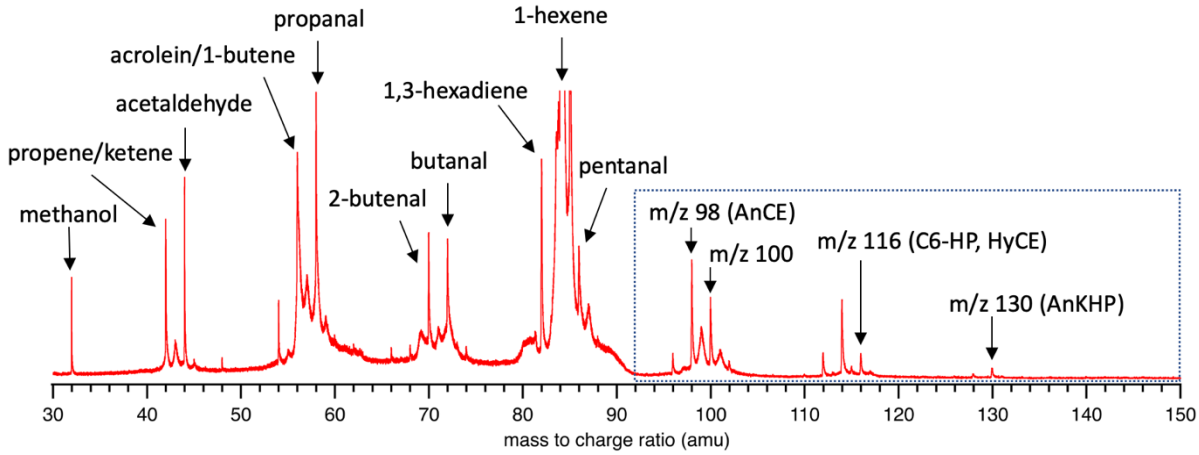

Figure 2. Typical time-of-flight mass spectrum obtained by integration over the photon energy range from 8.5 to 10.5 eV with a step size of 10 meV and an acquisition time of 60 s per step during the LTO of 1-hexene at ϕ = 0.5 and T = 625 K. The dashed box shows the region of interest in this work. The vertical scale is reduced to zoom out the low intensity peaks so that 1-hexene (m/z 84) and its ^{13}C isotopomer (m/z 85) are cut off. In contrast to the indicated m/z values, the given chemical names related to an unambiguous identification of the isomers.

The mass spectrum obtained during the LTO of 1-hexene at ϕ = 0.5 and T = 625 K is displayed in Figure 2. The spectrum identifies some of the primary intermediates reported in the literature, with m/z = 130 being the highest mass detected and m/z = 32 the lowest. The predominant signal at m/z = 84 corresponds to 1-hexene, while decomposition products (with fewer than 6 carbons) and oxidized products (6 carbon atoms with one or more oxygen atoms) are present in the spectrum with a good signal-to-noise ratio. Although the highest oxidized product at m/z = 130 (AnKHP, $C_6H_{10}O_3$) has a weak signal, it is still visible. However, no signal could be observed at m/z = 148 (HyKHP, $C_6H_{12}O_4$). The dashed box in Figure 2 highlights the area of interest in this study.

In Figure 3, the TPES of m/z = 116 is compared with a simulated spectrum of the trans configuration of (5-methyltetrahydrofuran-2-yl)methanol (HyCE). The experimental TPES displays a noticeable ionization threshold around 9 eV. The previous study by Battin-Leclerc et al. [3] reported an ionization threshold of m/z = 116 around 9.2 eV based on the TIY curve. However, upon closer inspection, a signal is already present at 9.0 eV in their reported TIY of m/z = 116. Table S1 presents the calculated AIEs of the expected isomers of m/z = 116 for the lowest-energy conformer compared to previous calculations from Battin-Leclerc et al. [3]. The two sets of calculations are in good agreement. The AIE of HyCE is the only one compatible with the measured ionization threshold of m/z = 116. All other isomers have AIEs above a reasonable value for the accuracy of the present calculations, 9.1 eV, including 3-hydroperoxyhex-1-ene (C6-HP) for which 70 conformers have been considered in this work,

having AIEs within a 318 meV range (9.06 – 9.38 eV). The simulated spectrum of HyCE, agrees well with the experimental spectrum, indicating that it is the dominant isomer at m/z = 116. Although the prevailing isomer at m/z = 116 is seemingly HyCE, the existence of other isomers cannot be ruled out in this work.

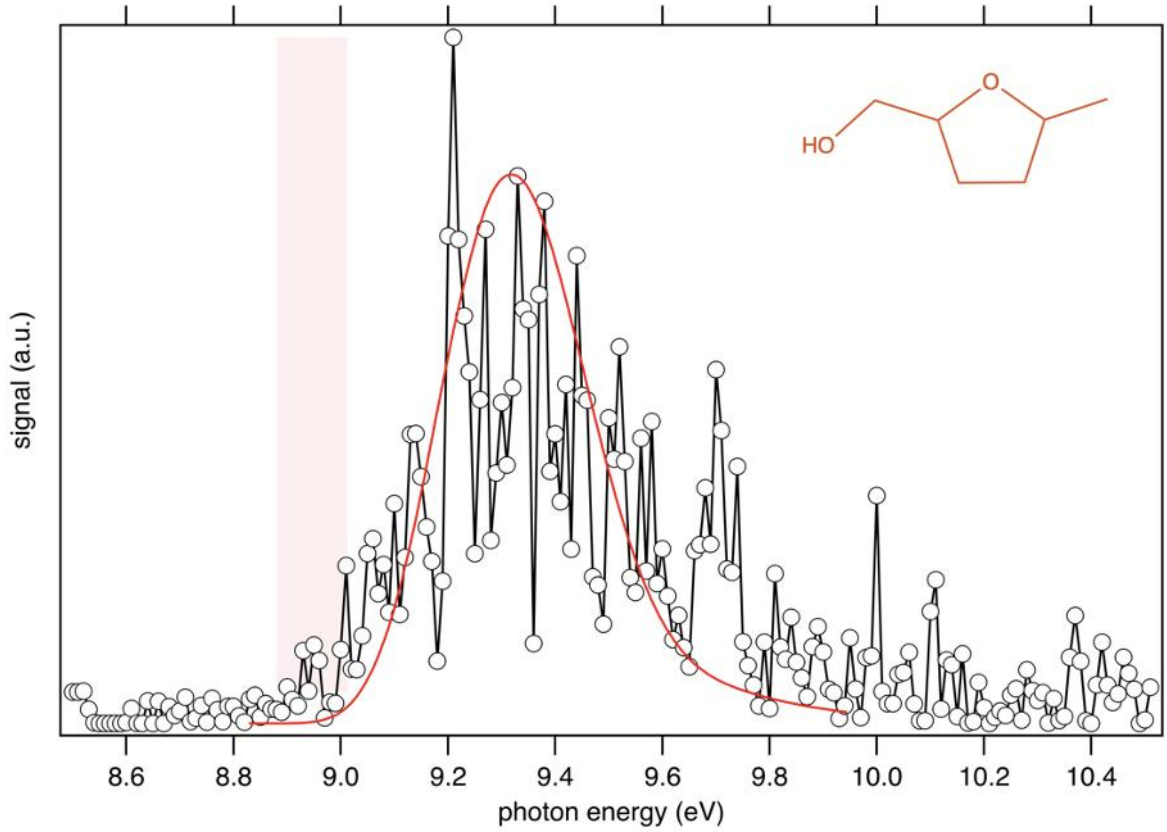

Figure 3. TPES of m/z 116 (open dots) compared to a simulated spectrum of the lowest energy neutral conformer of 5-methyltetrahydrofuran-2-yl)methanol (red line). The red shaded region shows the conformer-dependent AIE of the HyCE.

In this work, to convert the normalized ion signal of a given species *i* to its mole fraction at a specific temperature, the fuel was used as an internal standard [25]. The fuel mole fraction value under the current conditions ($\phi = 0.5$ and T = 625 K) was taken from Meng et al. [4], and its PICS at 10.6 eV from Yang et al. [38]. When a molecule is ionized, the total charge on the produced ions equals the charge of the parent molecule. Therefore, the sum of the signals from all fragments and that of the parent must equal the total signal intensity. This relationship allows the use of a fragment signal to determine the concentration of a given species, as the signal of a fragment is proportional to the concentration of the parent

molecule. When one of the fragments has a distinct m/z and a relatively good signal-to-noise ratio, the mole fraction of the species of interest can be calculated using the following equation [39]:

$$x_i(T) = x_{fuel}(T) \cdot \frac{S_i(T,E)}{S_{fuel}(T,E)} \cdot \frac{\sigma_{fuel}(E)}{\sigma_i(E)} \cdot \frac{D_{fuel}}{D_p} \cdot \frac{\rho_{fuel}}{\rho_i}$$

Here, $x_i(T)$, $S_i(T,E)$, $\sigma_i(E)$, and $\rho_i(E)$ represent the mole fraction, signal, PICS, and transmission factor of species *i* or one of its fragments at photon energy *E* and temperature *T,* respectively. For compounds where the PICS is not available in the literature, an estimate was made using the group additivity method proposed by Bobeldijk et al. [40], in which groups are defined as atom pairs in the considered molecules. The value of each group was estimated from published data of known species at the given photon energy. Note this method only provides an estimate of the total PICS. In this work, the values of each group at 10.6 eV were summed to constitute the related molecule, thereby estimating the PICS. Table S2 provides the list of the estimated PICS at 10.6 eV used for quantifying species in this study. D_p is the mass discrimination factor of the neutral parent *p* of ion *i* until it reaches the ionization region. The transmission factor ρ_i in coincidence experiments, refers to the combined efficiency of electrons and ions passing through the VMI and time-of-flight mass analyzer, respectively. With the 88 V/cm extraction field applied in this work, the electrons are fully transmitted up to 3.5 eV kinetic energy and ion transmission is independent of mass [41]. Additionally, it is important to note that with an ion impact energy of 3.8 kV and within the mass range investigated in this study, any mass effects on ion detection efficiency are anticipated to be minimal.

A weak signal is detected at m/z 83, which could be attributed to a fragment $C_6H_{11}^+$ ion resulting from the dissociative ionization of C6-HP. Hydroperoxides are known to undergo fragmentation upon photoionization, mainly by losing an OOH group [21]. Assuming no other contribution to m/z 83, C6-HP can be quantified under the specific conditions of $\phi = 0.5$ and T = 625 K using the peak area at m/z 83 in the registered mass spectra and its partial PICS, estimated to be 13.5 Mb at a photon energy of 10.6 eV using Bobeldijk's method [40]. Figure 4 compares the mole fraction of C6-HP from this work with the prediction of a detailed kinetic model from Nancy [4]. The results in this work were also

compared to the experimental data of Meng et al. [4]. It is worth noting that simulation results for the kinetic model from Galway [6] are not reported, due to its poor agreement with experiments for the equivalence ratio of 0.5 used in this work. The mole fraction of 7×10^{-6} for C6-HP obtained in this work at 625 K is in excellent agreement with the predictions of the kinetic model from Nancy, especially considering the discrepancy factor of 6 previously reported in the literature between experiments and simulations [4].

Considering that the signal at m/z 116 is mainly due to HyCE, its mole fraction was calculated using the peak area of m/z 116, and by taking 16.7 Mb as its partial PICS using Bobeldijk's method [40]. The mole fraction agrees within a factor of 2 with the previous mole fraction from Meng et al. [4] (see Figure 4). The C6-HP/HyCE mole fraction ratio of 0.2 ± 0.1 obtained in this work is in line with the predicted mole fraction ratio of 0.1 using the kinetic model from Nancy [4].

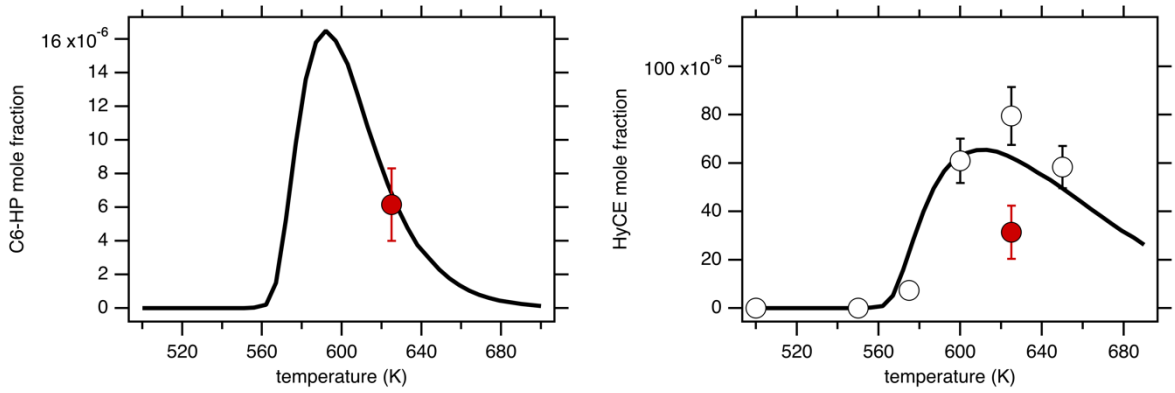

Figure 4. Comparison of the calculated mole fraction of C6-HP (left) and HyCE (right) from the kinetic model from Nancy [4] (black line), the GC experimental measurements of Meng et al. [4] (open dots), and the experimental measurements from this work (red dots).

Figure 5 illustrates the comparison between the TPES of m/z 130 obtained and the simulated spectra of AnKHP isomers. The ionization threshold is around 8.9 eV, slightly lower than the value reported by Xie et al. [8]. However, there is a small signal below 9.0 eV visible in the TIY curve of m/z 130. Despite a low signal-to-noise ratio, the experimental TPES of m/z 130 is relatively well-fitted by a convolution of the simulated PES of the lowest-energy conformers of 5-hydroperoxyhexen-3-one and 3-hydroperoxyhexen-5-one. The fit yields a 5-hydroperoxyhexen-3-one:3-hydroperoxyhexen-5-one signal ratio of 1.0 ± 0.2 : 1.0 ± 0.2 within a 2σ confidence interval (see Figure 5), after moderately shifting the

simulated spectra by ~30 and ~70 meV from their respective calculated AIE at the CBS-QB3 level of theory.

By assuming a similar PICS for both isomers, the ratio derived from experimentation is higher than the predicted mole fraction ratios of 1:0.5 and 1:0.2 from the kinetic models of Nancy [4] and Galway [6], respectively. It is worth noting that this comparison assumes equal transition strength between the isomers and neglects the effects that autoionization might have on the different isomers . As mentioned in the theoretical methods, weak FC overlap integrals between the vibrational ground states of the initial and final states introduce a level of uncertainty that affects the reliability of the results. Nevertheless, the underprediction of 5-hydroperoxyhexen-3-one's presence aligns with the experimental observations made by Xie et al. [8].

Furthermore, because of the flexible structure of AnKHP isomers, a rigorous conformer analysis was performed using electronic structure calculations at the M06-2X-D3/aug-cc-pVTZ level of theory. Figure S1 shows a conformational analysis performed for the AnKHP isomer, 3-hydroperoxyhexen-5-one, revealing that its lowest-energy conformer has a calculated AIE lower by 350 meV than the value reported by Xie et al. [8]. Using this level of theory, 45 conformers were analyzed, and the maximum AIE difference among them was found to be 1.35 eV (8.26 – 9.61 eV).

The structure analysis identified 33 neutral 5-hydroperoxyhexen-3-one conformers, and their AIE, electronic energy, and expected Boltzmann fractions at T = 625 K are summarized in Figure S2. The analysis revealed that the maximum AIE difference among the conformers is 0.9 eV (8.83 – 9.73 eV). Out of the 33 conformers, three have small energy difference (less than 50 meV), and the two lowest-energy conformers have almost the same energy but distinct structures and AIE (see Figure S2). The lowest-energy conformer has an AIE that agrees well with the value reported by Xie et al. [8]. However, when performing FCF simulations, it was observed that the simulated spectrum of the second lowest-energy conformer of 5-hydroperoxyhexen-3-one overlaps with the simulated spectrum of the lowest-energy conformer of 3-hydroperoxyhexen-5-one. By substituting the simulating spectrum of 3-hydroperoxyhexen-5-one with that of the second lowest-energy conformer of 5-hydroperoxyhexen-3-one, a similar fit with a ratio of $1.0 \pm 0.2 : 1.0 \pm 0.1$ as shown in Figure 5 can be achieved (see Figure S3). This indicates that providing an accurate ratio of 5-hydroperoxyhexen-3-one to 3-hydroperoxyhexen-5-one is challenging due to potential

contributions from different conformers of 5-hydroperoxyhexen-3-one and a low signal-to-noise ratio.

A comparison between the integral of the simulated spectra shown in Figure 5 and the TIY of m/z 130 is provided in the SM (see Figure S4). The weighted fit using the integral of the simulated spectra of 5-hydroperoxyhexen-3-one and 3-hydroperoxyhexen-5-one leads to a signal ratio of 1.0 : 1.0, similar to the one found in the TPES analysis of Figure 5. Thus, it can be confidently stated that the predictions of the kinetic models in the literature underestimate the presence of 5-hydroperoxyhexen-3-one.

In the kinetic model from Nancy [4], the rate constants for the reaction 1-hexene + OH are set equal to the values suggested by Zádor et al. [42] for propene. When it comes to 1-hexene, this reaction forms allylic radicals (E) which eventually produce AnKHP (see Figure 1). The rate constant of H-abstraction from the CH_2 group closest to the unsaturated bond forms hex-1-en-3-yl which leads to 5-hydroperoxyhexen-3-one. However, this H-abstraction reaction is slower than the formation of hex-1-en-5-yl leading to 3-hydroperoxyhexen-5-one. However, our calculations at the CBS-QB3 level of theory indicate that the energy required to break the bond is about 20% less when abstracting hydrogen from the CH_2 group closest to the unsaturation than from the secondary C-H bond site. It could be valuable to individually assess the rate constants of the hexene and OH reaction to determine if this could account for the observed underestimation of 5-hydroperoxyhexen-3-one. This should be done in combination with an inspection of the kinetics of hex-1-en-3-yl + HO2, which is the main sink of this allylic radical. An important overprediction of the decomposition products from hex-1-en-3-yl + HO2 (unsaturated aldehydes such as hexenal and acrolein) has been shown in Meng et al. [4].

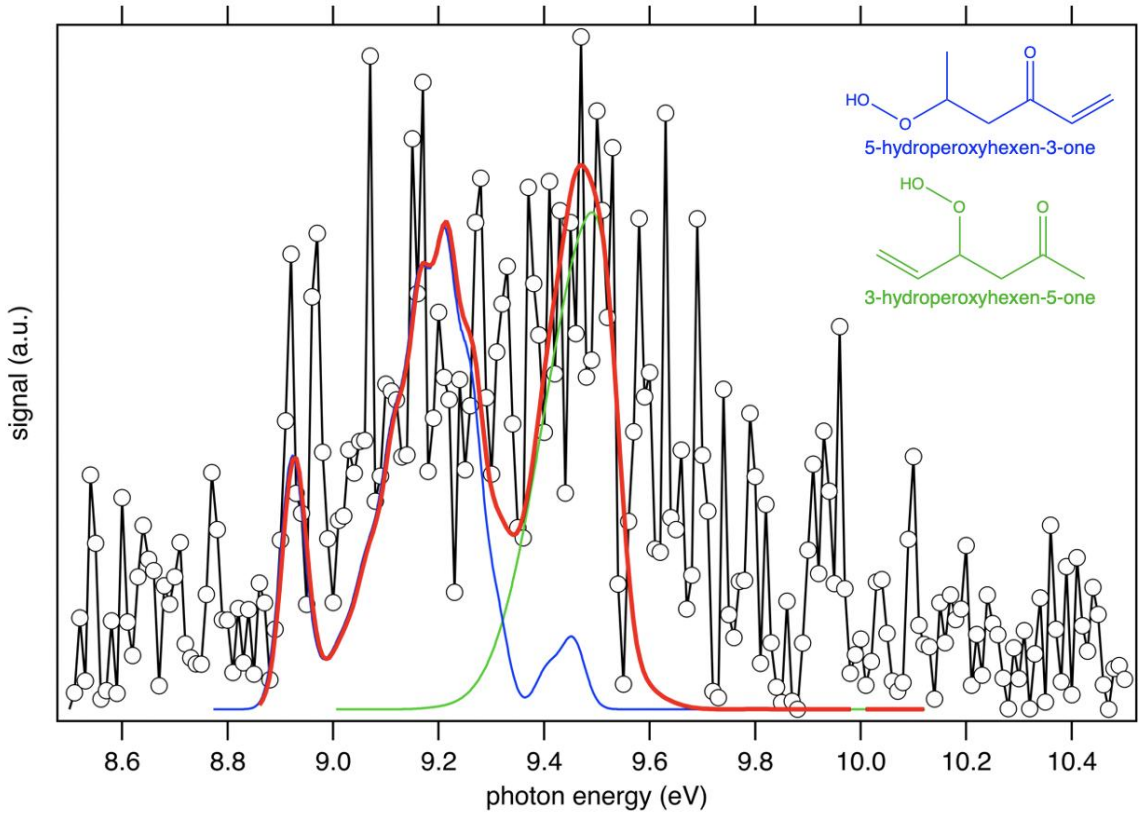

Figure 5. TPES of m/z 130 (open dots) compared to simulated spectra of the lowest-energy conformer of 5-hydroperoxyhexen-3-one (blue line) and 3-hydroperoxyhexen-5-one (green line). The thick red line is the result of a weighted fit (see text for details).

In the current work, no signal was detected at m/z 148 for HyKHP ($C_6H_{12}O_4$). This lack of detection can be attributed to a lower sensitivity compared to the study by Xie et al. [8]. In their study, the signal ratio between m/z 130 and m/z 148 indicated that m/z 148 was 15 times lower than m/z 130, causing the signal to be overshadowed by noise in the registered mass spectra of the current work. Additionally, the temperature used in the current experiment (625 K) was slightly higher than the temperature used in Xie et al.'s study [8] (600 K). According to the kinetic model found in the literature, this lower working temperature in the study by Xie et al. [8] favors the formation of HyKHP over AnKHP.

Therefore, the theoretical calculations on HyKHP isomers performed in this work are used to analyze the TIY curve of m/z 148 presented in Xie et al. [8]. The addition of a hydroxyl group made the analysis of HyKHP isomers more challenging, resulting in the calculation of over 100 conformers for each of the four isomers considered in Xie et al. [8]. Table S3 compares the AIE calculated by Xie et al. [8] with those calculated in this study, and strong

disagreements were found between the two sets of calculations for all isomers, except for 4-hydroperoxy-2-hydroxyhexan-1-one.

According to our analysis, 4-hydroperoxy-1-hydroxyhexan-2-one, the most abundant isomer predicted by kinetic models in the literature, is the only one whose AIE matches the TIY ionization threshold of m/z 148 estimated at 9.20 eV in Xie et al. [8]. Additionally, the simulated TIY obtained by integration of the calculated FCF of 4-hydroperoxy-1-hydroxyhexan-2-one matches the beginning of the TIY curve well (see Figure 6). Therefore, it is possible to conclude, based on available data, that 4-hydroperoxy-1-hydroxyhexan-2-one is the dominant HyKHP isomer, this conclusion is in agreement with the predictions of the kinetic model.

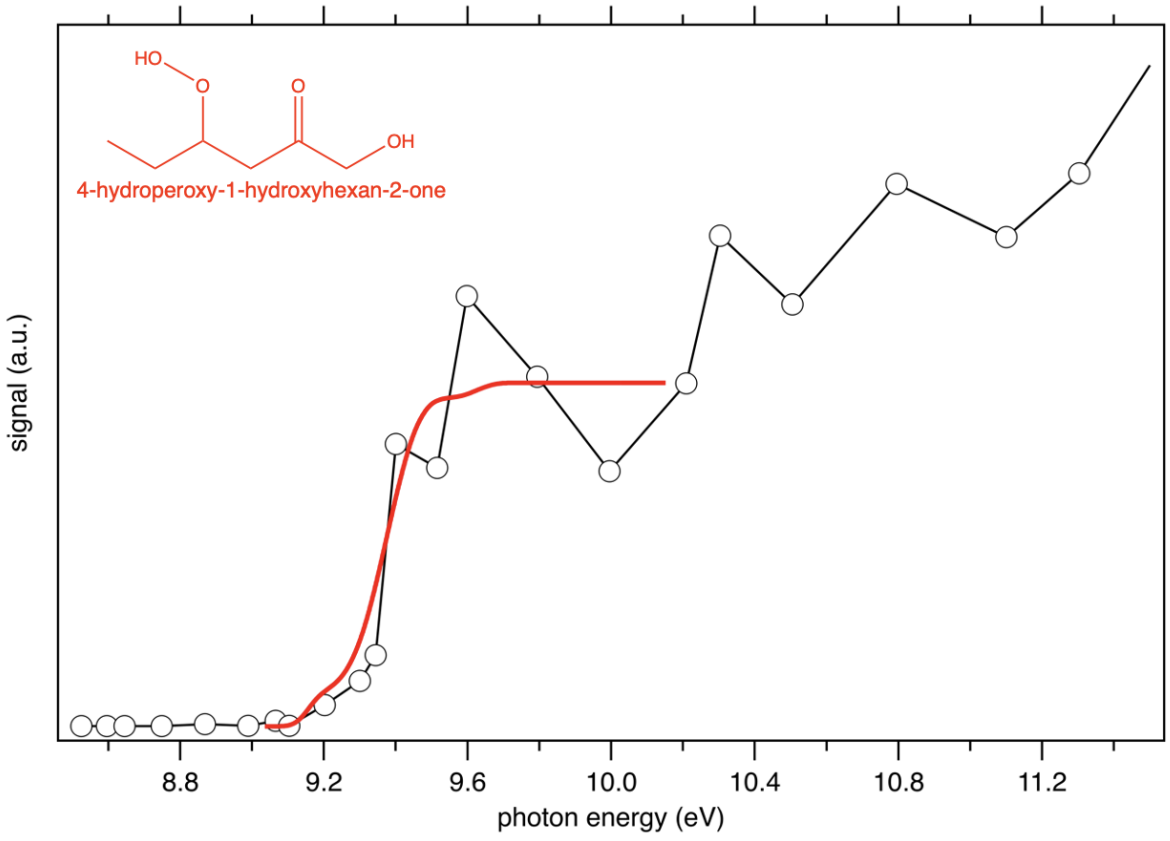

Figure 6. TIY curve of m/z 148 (open dots) from Xie et al. compared to a simulated spectrum of 4-hydroperoxy-1-hydroxyhexan-2-one (red line).

In this study, AnKHP and HyKHP were quantified at 625 K using the same quantification method previously applied to C6-HP and HyCE. The quantification of AnKHP was performed using the peak area of m/z 130, with the assumption of no significant fragmentation upon photoionization. The lack of a peak at m/z 97, which would have matched a $C_6H_9O^+$ fragment

resulting from AnKHP fragmentation with HO_2-loss, supports this assumption. The total PICS of $C_6H_{10}O_3$ was estimated to be 25.2 Mb at a photon energy of 10.6 eV, and this value was used in the quantification of AnKHP.

As for HyKHP, no peak was detected at m/z 148, but a signal was observed at m/z 115, corresponding to the loss of an HO_2 group from HyKHP. It is worth noting that the higher temperature used in this study might have caused increased fragmentation of the m/z 148 ion, contributing to its non-detection in the current mass spectra. This phenomenon could also explain why m/z 148 was not identified. The signal of m/z 115 was utilized to quantify HyKHP, assuming a partial PICS of a $C_6H_{11}O_2^+$ fragment, estimated to be 12.3 Mb at 10.6 eV.

Experimental results revealed an AnKHP/HyKHP ratio of 2.5 $\pm$ 1.2 at 625 K, aligning well with the ratio of 4.1 by Xie et al. [43] at 600 K. When compared with the predictions from the kinetic model provided by Nancy [4], it was confirmed that the AnKHP/HyKHP ratio is underpredicted. The discrepancy can be visualized in Figure 7 (right), illustrating the comparison between experimental findings and model predictions.

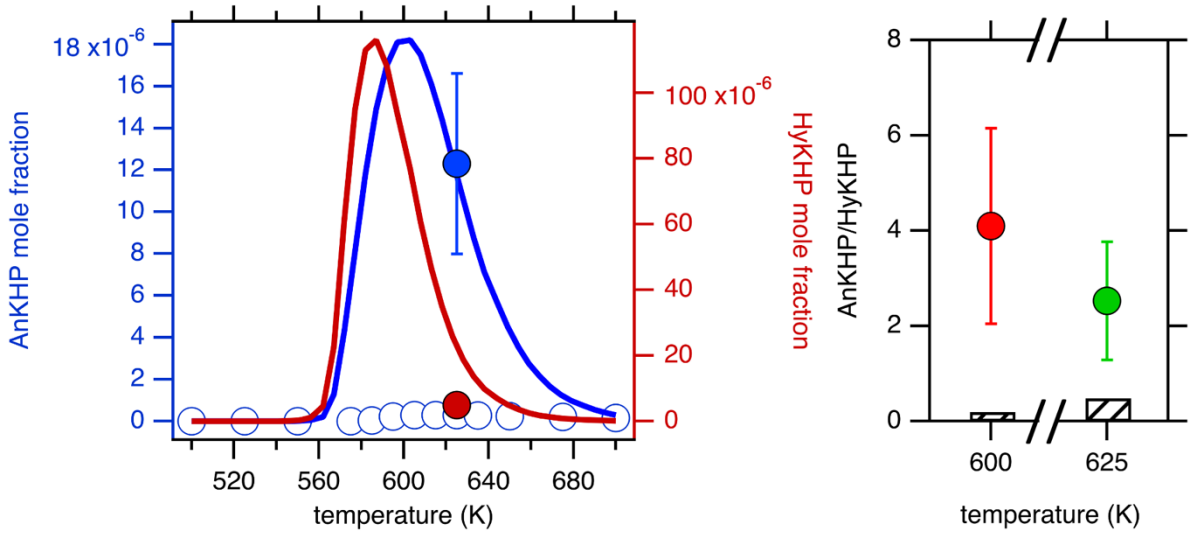

Figure 7. (left) Simulated mole fraction profile (lines) of AnKHP (blue) and HyKHP (red) from the kinetic model of Nancy [4] compared to the experimental mole fraction measured in this work (full dots) and by MS in Meng et al. [4] (open dots) ; (right) Experimental AnKHP/HyKHP ratio at 600 K from Xie et al.[8] (red dots) and at 625 K from this work (green dots) compared to the predictions of the kinetic model from Nancy (bars) [4].

Figure 7 (left) displays the experimental mole fraction of AnKHP at 625 K. This result aligns well with the predictions from the kinetic model by Nancy [4], yielding a value of 12 ppm. However, the same model falls short according to the findings of Meng et al. [4], who reported an underestimation by a factor of 25.

Interestingly, Figure 7 (left) also highlights an overprediction by the model for HyKHP, overestimating it by a factor of 5. This discrepancy contributes to the higher observed experimental between AnKHP and HyKHP, as depicted in Figure 7 (right).

These findings reinforce the observations made by Xie et al. [8], the chain branching pathway through the formation of AnKHP dominates the low-temperature chemistry, contrary to the predictions from the kinetic models in the literature.

Xie et al. [8] speculated that the discrepancy might be linked to the competition between two chemical mechanisms: the Waddington reaction and the chain branching process through HyKHP. Stark and Waddington [17] previously suggested a reaction pathways involving hydroxyperoxyradicals that leads to the formation of radicals and aldehydes, like pentanal (m/z 86).

The experimental mole fraction of pentanal at 625 K, depicted in Figure 8 (left), is 119 ppm. While this is overpredicted by a factor of 3.5 by the kinetic model, it aligns with previous experimental data from Meng et al. [4]. This overprediction applies to both pentanal and HyKHP.

However, it's important to recognize that simply reevaluating the branching ratio of the Waddington channel and the HyKHP chain branching channel may not resolve the inconsistency between the simulations and experimental results concerning the AnKHP/HyKHP ratio. This realization suggests that more detailed and nuanced understanding may be required to bridge the gap between theory and experimental observation.

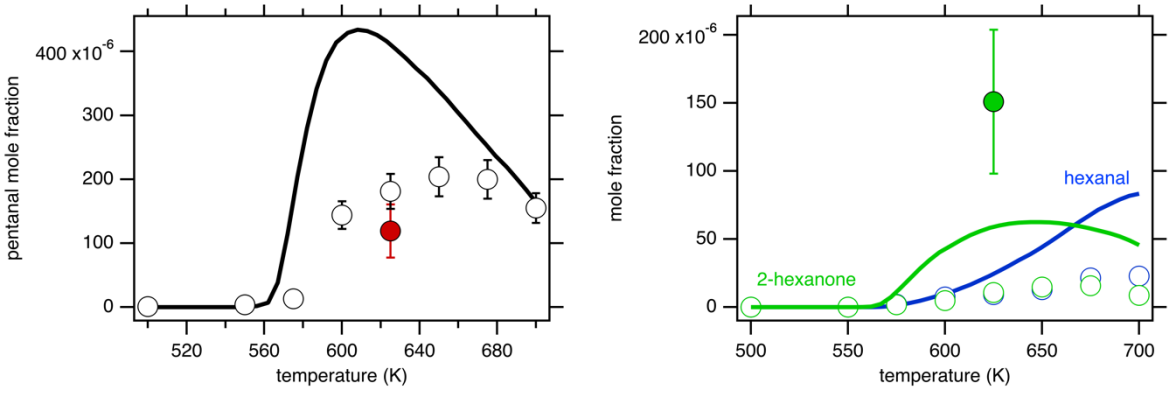

Figure 8. (left) Simulated mole fraction profile (black line) of pentanal from the kinetic model of Nancy [4] compared to the experimental mole fraction calculated in this work (red dot) and from Meng et al. [4] (open dots) ; (right) Simulated mole fraction profile (line) of hexanal (blue) and 2-hexanone (green) from the kinetic model of Nancy [4] compared to the experimental mole fraction measured in this work (green dot) and GC ones from Meng et al. [4] (open dots).

Hydroxy alkyl radicals (ROH) produced by the OH-addition to 1-hexene have two main pathways: they can react with molecular oxygen or undergo a two-step isomerization process, as shown in Figure 1. The isomerization has an inhibiting effect because it can lead to the creation of unreactive HO_2 radicals, hexanal, and 2-hexanone (m/z 100).

When comparing the predicted mole fraction of hexanal and 2-hexanone with experimental data, the kinetic model seems to overpredict these values (see Figure 8 (right)). In this particular study, the experimental mole fraction of 2-hexanone was measured at 151 ppm at 625 K, which not only contrasts with previous experimental values but is also underpredicted by nearly a factor of 3 (see Figure 8).

Unfortunately, the formation of hexanal couldn't be thoroughly analyzed in this study because it overlaps structurally with 2-hexanone (as referenced in Figure S5). However, previous experimental mole fractions of hexanal have also been found to be slightly overpredicted by the kinetic model.

These inconsistencies suggest that a reevaluation of the branching ratio between the isomerization and O_2-addition of ROH radicals might be necessary. According to a reaction flux analysis using the kinetic model from Nancy, the O_2-addition reaction currently seems to be ten times faster than the isomerization towards hexan-2-one. This discrepancy might be an underlying reason for the overprediction of HyKHP and warrants further investigation to align the kinetic model with experimental observations.

CONCLUSION

In this study, the SVUV-PEPICO technique was employed for the first time to investigate 1-hexene LTO in a near-atmospheric JSR at a fixed temperature of 625 K and an equivalence ratio of 0.5. The isomeric structures of the primary hydroperoxides, cyclic ethers, and ketohydroperoxides were refined, with a thorough study of the conformational landscape, and their experimental mole fractions were compared to predictions from a kinetic model found in the literature.

The results indicate that existing kinetic models inaccurately predict the formation of HyKHP. However, the current work demonstrates that the formation of AnKHP, along with the ratio of unsaturated C6 hydroperoxides to HyCE, aligns closely with model predictions. It can, therefore, be concluded that the overprediction of HyKHP is not due to the branching ratio

between H-atom abstraction and OH radical addition reactions on 1-hexene or the competition between the Waddington mechanism and the chain branching process through HyKHP. Conversely, the model appears to underestimate the formation of 2-hexanone, a product of the isomerization of ROH radicals. This finding suggests that reevaluating the branching ratio of these radicals might resolve the discrepancy between the model's predictions and the experimental data concerning the AnKHP/HyKHP ratio.

ACKNOWLEDGEMENT

We acknowledge SOLEIL for provision of synchrotron radiation under project 20210964 and we are grateful to J.-F. Gil for his technical help around the SAPHIRS set-up. We thank the QUADMARTS International Research Network for promoting the collaboration. This work was performed using HPC resources from the EXPLOR centre hosted by the University of Lorraine (Project: 2021EXTXX2356).

REFERENCES

[1] J. Wang, B. Yang, Y. Li, Z. Tian, T. Zhang, F. Qi, K. Nakajima, The tunable VUV single-photon ionization mass spectrometry for the analysis of individual components in gasoline, International Journal of Mass Spectrometry. 263 (2007) 30–37. https://doi.org/10.1016/j.ijms.2006.12.005.

[2] R. Bounaceur, V. Warth, B. Sirjean, P.A. Glaude, R. Fournet, F. Battin-Leclerc, Influence of the position of the double bond on the autoignition of linear alkenes at low temperature, Proceedings of the Combustion Institute. 32 (2009) 387–394. https://doi.org/10.1016/j.proci.2008.05.009.

[3] F. Battin-Leclerc, A. Rodriguez, B. Husson, O. Herbinet, P.-A. Glaude, Z. Wang, Z. Cheng, F. Qi, Products from the Oxidation of Linear Isomers of Hexene, J. Phys. Chem. A. 118 (2014) 673–683. https://doi.org/10.1021/jp4107102.

[4] X. Meng, A. Rodriguez, O. Herbinet, T. Wang, F. Battin-Leclerc, Revisiting 1-hexene low-temperature oxidation, Combustion and Flame. 181 (2017) 283–299. https://doi.org/10.1016/j.combustflame.2017.03.031.

[5] Y. Wu, Y. Liu, C. Tang, Z. Huang, Ignition delay times measurement and kinetic modeling studies of 1-heptene, 2-heptene and n-heptane at low to intermediate temperatures by using a rapid compression machine, Combustion and Flame. 197 (2018) 30–40. https://doi.org/10.1016/j.combustflame.2018.07.007.

[6] S. Dong, C. Aul, C. Gregoire, S.P. Cooper, O. Mathieu, E.L. Petersen, J. Rodriguez, F. Mauss, S.W. Wagnon, G. Kukkadapu, W.J. Pitz, H.J. Curran, A comprehensive experimental and kinetic modeling study of 1-hexene, Combustion and Flame. 232 (2021) 111516. https://doi.org/10.1016/j.combustflame.2021.111516.

[7] C. Cao, X. Zhang, Y. Zhang, J. Zou, Y. Li, J. Yang, F. Qi, Probing the fuel-specific intermediates in the low-temperature oxidation of 1-heptene and modeling interpretation, Proceedings of the Combustion Institute. 38 (2021) 385–394. https://doi.org/10.1016/j.proci.2020.06.025.

[8] C. Xie, Q. Xu, W. Chen, T. Yu, L. Wei, L. Xing, Z. Wang, Evaluating the role of hydroxyl keto-hydroperoxide in the low temperature oxidation of alkenes, Combustion and Flame. 246 (2022) 112414. https://doi.org/10.1016/j.combustflame.2022.112414.

[9] G. Vanhove, M. Ribaucour, R. Minetti, On the influence of the position of the double bond on the low-temperature chemistry of hexenes, Proceedings of the Combustion Institute. 30 (2005) 1065–1072. https://doi.org/10.1016/j.proci.2004.08.042.

[10] N. Lokachari, G. Kukkadapu, H. Song, G. Vanhove, M. Lailliau, G. Dayma, Z. Serinyel, K. Zhang, R. Dauphin, B. Etz, S. Kim, M. Steglich, A. Bodi, G. Fioroni, P. Hemberger, S.S. Matveev, A.A. Konnov, P. Dagaut, S.W. Wagnon, W.J. Pitz, H.J. Curran, A comprehensive experimental and kinetic modeling study of di-isobutylene isomers: Part 1, Combustion and Flame. 251 (2023) 112301. https://doi.org/10.1016/j.combustflame.2022.112301.

[11] G. Vanhove, G. Petit, R. Minetti, Experimental study of the kinetic interactions in the low-temperature autoignition of hydrocarbon binary mixtures and a surrogate fuel, Combustion and Flame. 145 (2006) 521–532. https://doi.org/10.1016/j.combustflame.2006.01.001.

[12] M. Mehl, G. Vanhove, W.J. Pitz, E. Ranzi, Oxidation and combustion of the n-hexene isomers: A wide range kinetic modeling study, Combustion and Flame. 155 (2008) 756–772. https://doi.org/10.1016/j.combustflame.2008.07.004.

[13] S. Touchard, R. Fournet, P.A. Glaude, V. Warth, F. Battin-Leclerc, G. Vanhove, M. Ribaucour, R. Minetti, Modeling of the oxidation of large alkenes at low temperature,

582 Proceedings of the Combustion Institute. 30 (2005) 1073–1081.
583 https://doi.org/10.1016/j.proci.2004.07.004.
584 [14] M. Yahyaoui, N. Djebaïli-Chaumeix, C.-E. Paillard, S. Touchard, R. Fournet, P.A.
585 Glaude, F. Battin-Leclerc, Experimental and modeling study of 1-hexene oxidation behind
586 reflected shock waves, Proceedings of the Combustion Institute. 30 (2005) 1137–1145.
587 https://doi.org/10.1016/j.proci.2004.08.070.
588 [15] M. Mehl, W.J. Pitz, C.K. Westbrook, K. Yasunaga, C. Conroy, H.J. Curran, Autoignition
589 behavior of unsaturated hydrocarbons in the low and high temperature regions, Proceedings
590 of the Combustion Institute. 33 (2011) 201–208.
591 https://doi.org/10.1016/j.proci.2010.05.040.
592 [16] M. Yahyaoui, N. Djebailichaumeix, P. Dagaut, C. Paillard, S. Gail, Kinetics of 1-hexene
593 oxidation in a JSR and a shock tube: Experimental and modeling study, Combustion and
594 Flame. 147 (2006) 67–78. https://doi.org/10.1016/j.combustflame.2006.07.011.
595 [17] M.S. Stark, D.J. Waddington, Oxidation of propene in the gas phase, Int. J. Chem.
596 Kinet. 27 (1995) 123–151. https://doi.org/10.1002/kin.550270205.
597 [18] F. Battin-Leclerc, J. Bourgalais, Z. Gouid, O. Herbinet, G. Garcia, P. Arnoux, Z. Wang,
598 L.-S. Tran, G. Vanhove, L. Nahon, M. Hochlaf, Chemistry deriving from OOQOOH radicals in
599 alkane low-temperature oxidation: A first combined theoretical and electron-ion coincidence
600 mass spectrometry study, Proceedings of the Combustion Institute. 38 (2021) 309–319.
601 https://doi.org/10.1016/j.proci.2020.06.159.
602 [19] J. Huang, C. Huang, Q. Hou, M. Wu, X. Wu, Y. Zhang, G. Tian, F. Zhang, A theoretical
603 study on dissociative photoionization and photoionization cross-sections of a typical
604 ketohydroperoxide in n-butane low-temperature oxidation, Combustion and Flame. (2022)
605 112490. https://doi.org/10.1016/j.combustflame.2022.112490.
606 [20] M. Demireva, K. Au, L. Sheps, Direct time-resolved detection and quantification of
607 key reactive intermediates in diethyl ether oxidation at *T* = 450–600 K, Phys. Chem. Chem.
608 Phys. 22 (2020) 24649–24661. https://doi.org/10.1039/D0CP03861J.
609 [21] Z. Hu, Q. Di, B. Liu, Y. Li, Y. He, Q. Zhu, Q. Xu, P. Dagaut, N. Hansen, S.M. Sarathy, L.
610 Xing, D.G. Truhlar, Z. Wang, Elucidating the photodissociation fingerprint and quantifying the
611 determination of organic hydroperoxides in gas-phase autoxidation, Proc. Natl. Acad. Sci.
612 U.S.A. 120 (2023) e2220131120. https://doi.org/10.1073/pnas.2220131120.
613 [22] I. Fischer, S.T. Pratt, Photoelectron spectroscopy in molecular physical chemistry,
614 Phys. Chem. Chem. Phys. 24 (2022) 1944–1959. https://doi.org/10.1039/D1CP04984D.
615 [23] P. Hemberger, A. Bodi, T. Bierkandt, M. Köhler, D. Kaczmarek, T. Kasper,
616 Photoelectron Photoion Coincidence Spectroscopy Provides Mechanistic Insights in Fuel
617 Synthesis and Conversion, Energy Fuels. 35 (2021) 16265–16302.
618 https://doi.org/10.1021/acs.energyfuels.1c01712.
619 [24] J. Bourgalais, Z. Gouid, O. Herbinet, G.A. Garcia, P. Arnoux, Z. Wang, L.-S. Tran, G.
620 Vanhove, M. Hochlaf, L. Nahon, Isomer-sensitive characterization of low temperature
621 oxidation reaction products by coupling a jet-stirred reactor to an electron/ion coincidence
622 spectrometer: case of n-pentane, Physical Chemistry Chemical Physics. 22 (2020) 1222–
623 1241.
624 [25] J. Bourgalais, O. Herbinet, H.-H. Carstensen, J. Debleza, G.A. Garcia, P. Arnoux, L.S.
625 Tran, G. Vanhove, B. Liu, Z. Wang, M. Hochlaf, L. Nahon, F. Battin-Leclerc, Jet-Stirred Reactor
626 Study of Low-Temperature Neopentane Oxidation: A Combined Theoretical,
627 Chromatographic, Mass Spectrometric, and PEPICO Analysis, Energy Fuels. 35 (2021) 19689–
628 19704. https://doi.org/10.1021/acs.energyfuels.1c02080.

[26] J. Bourgalais, H.-H. Carstensen, O. Herbinet, G.A. Garcia, P. Arnoux, L.-S. Tran, G. Vanhove, L. Nahon, M. Hochlaf, F. Battin-Leclerc, Product Identification in the Low-Temperature Oxidation of Cyclohexane Using a Jet-Stirred Reactor in Combination with SVUV-PEPICO Analysis and Theoretical Quantum Calculations, The Journal of Physical Chemistry A. 126 (2022) 5784–5799. https://doi.org/10.1021/acs.jpca.2c04490.
[27] X. Tang, G.A. Garcia, J.-F. Gil, L. Nahon, Vacuum upgrade and enhanced performances of the double imaging electron/ion coincidence end-station at the vacuum ultraviolet beamline DESIRS, Review of Scientific Instruments. 86 (2015) 123108. https://doi.org/10.1063/1.4937624.
[28] L. Nahon, N. de Oliveira, G.A. Garcia, J.-F. Gil, B. Pilette, O. Marcouillé, B. Lagarde, F. Polack, DESIRS: a state-of-the-art VUV beamline featuring high resolution and variable polarization for spectroscopy and dichroism at SOLEIL, J Synchrotron Rad. 19 (2012) 508–520. https://doi.org/10.1107/S0909049512010588.
[29] G.A. Garcia, B.K. Cunha de Miranda, M. Tia, S. Daly, L. Nahon, DELICIOUS III: A multipurpose double imaging particle coincidence spectrometer for gas phase vacuum ultraviolet photodynamics studies, Review of Scientific Instruments. 84 (2013) 053112. https://doi.org/10.1063/1.4807751.
[30] J.C. Poully, J.P. Schermann, N. Nieuwjaer, F. Lecomte, G. Grégoire, C. Desfrançois, G.A. Garcia, L. Nahon, D. Nandi, L. Poisson, M. Hochlaf, Photoionization of 2-pyridone and 2-hydroxypyridine, Phys. Chem. Chem. Phys. 12 (2010) 3566. https://doi.org/10.1039/b923630a.
[31] T.A. Halgren, MMFF VII. Characterization of MMFF94, MMFF94s, and other widely available force fields for conformational energies and for intermolecular-interaction energies and geometries, Journal of Computational Chemistry. 20 (1999) 730–748. https://doi.org/10.1002/(SICI)1096-987X(199905)20:7<730::AID-JCC8>3.0.CO;2-T.
[32] Y. Zhao, D.G. Truhlar, The M06 suite of density functionals for main group thermochemistry, thermochemical kinetics, noncovalent interactions, excited states, and transition elements: two new functionals and systematic testing of four M06-class functionals and 12 other functionals, Theor Chem Account. 120 (2008) 215–241. https://doi.org/10.1007/s00214-007-0310-x.
[33] R.A. Kendall, T.H. Dunning, R.J. Harrison, Electron affinities of the first-row atoms revisited. Systematic basis sets and wave functions, J. Chem. Phys. 96 (1992) 6796–6806. https://doi.org/10.1063/1.462569.
[34] S. Grimme, J. Antony, S. Ehrlich, H. Krieg, A consistent and accurate ab initio parametrization of density functional dispersion correction (DFT-D) for the 94 elements H-Pu, J. Chem. Phys. 132 (2010) 154104. https://doi.org/10.1063/1.3382344.
[35] J. Bloino, Aiming at an accurate prediction of vibrational and electronic spectra for medium-to-large molecules: An overview - Bloino - 2016 - International Journal of Quantum Chemistry - Wiley Online Library, (2016). https://onlinelibrary.wiley.com/doi/full/10.1002/qua.25188 (accessed June 7, 2021).
[36] J.A. Montgomery, M.J. Frisch, J.W. Ochterski, G.A. Petersson, A complete basis set model chemistry. VI. Use of density functional geometries and frequencies, J. Chem. Phys. 110 (1999) 2822–2827. https://doi.org/10.1063/1.477924.
[37] J.A. Montgomery, M.J. Frisch, J.W. Ochterski, G.A. Petersson, A complete basis set model chemistry. VII. Use of the minimum population localization method, J. Chem. Phys. 112 (2000) 6532–6542. https://doi.org/10.1063/1.481224.
[38] B. Yang, J. Wang, T.A. Cool, N. Hansen, S. Skeen, D.L. Osborn, Absolute

photoionization cross-sections of some combustion intermediates, International Journal of Mass Spectrometry. 309 (2012) 118–128. https://doi.org/10.1016/j.ijms.2011.09.006.
[39] T.A. Cool, J. Wang, K. Nakajima, C.A. Taatjes, A. Mcllroy, Photoionization cross sections for reaction intermediates in hydrocarbon combustion, International Journal of Mass Spectrometry. 247 (2005) 18–27. https://doi.org/10.1016/j.ijms.2005.08.018.
[40] M. Bobeldijk, W.J. van der Zande, P.G. Kistemaker, Simple models for the calculation of photoionization and electron impact ionization cross sections of polyatomic molecules, Chemical Physics. 179 (1994) 125–130. https://doi.org/10.1016/0301-0104(93)E0376-7.
[41] I. Derbali, H.R. Hrodmarsson, Z. Gouid, M. Schwell, M.-C. Gazeau, J.-C. Guillemin, M. Hochlaf, M.E. Alikhani, E.-L. Zins, Photoionization and dissociative photoionization of propynal in the gas phase: theory and experiment, Phys. Chem. Chem. Phys. 21 (2019) 14053–14062. https://doi.org/10.1039/C8CP06751A.
[42] J. Zádor, A.W. Jasper, J.A. Miller, The reaction between propene and hydroxyl, Phys. Chem. Chem. Phys. 11 (2009) 11040. https://doi.org/10.1039/b915707g.
[43] C. Xie, M. Lailliau, G. Issayev, Q. Xu, W. Chen, P. Dagaut, A. Farooq, S.M. Sarathy, L. Wei, Z. Wang, Revisiting low temperature oxidation chemistry of n-heptane, Combustion and Flame. 242 (2022) 112177. https://doi.org/10.1016/j.combustflame.2022.112177.